ADVANCED OPTICAL MATERIALS
www.advopticalmat.de

Self-Rolling SiO_2/Au Based Epsilon-Near-Zero Metamaterials

*Mohsin Habib, Ibrahim Issah, Esteban Bermúdez-Ureña, and Humeyra Caglayan**

Wave propagation in epsilon-near-zero (ENZ) media offers exciting possibilities in the field of nanophotonics. Here, a thin film self-rolling technique to fabricate SiO_2/Au based 3D multilayer structures is implemented. These cylindrical multilayer metamaterials are utilized to take advantage of the material dispersion as well as the structural dispersion to obtain self-rolling ENZ metamaterials at the visible to near-infrared wavelength range. The ENZ features are investigated initially by modelling the dispersion of the effective medium using circular effective medium approximation and further by the characterization of the optical response. Moreover, the potential of these structures for supporting an ENZ waveguide mode is demonstrated. This platform for dispersion engineering and obtaining ENZ metamaterials can provide opportunities for unique applications which cannot be possible with planar systems. It can be used to integrate active materials before the rolling process to actively control the layer properties, or embed single-layer materials within different layers of ENZ metamaterials with potential applications in quantum nanophotonics.

1. Introduction

Metamaterials as artificial engineered structures exhibit unconventional electromagnetic properties.[1] They have become important for enabling the engineering of novel electromagnetic properties in a variety of materials and the control of electromagnetic wave propagation in them.[2] By rationally arranging sub-wavelength structures, one can create designed effective media with prescribed dispersion and values of the electric permittivity (ε) and magnetic permeability (μ). The advancements in dispersion engineering provide the desired material response at different frequency ranges as well as additional functionalities such as loss control or photonic doping.[3] One class of metamaterials that have highly anisotropic and hyperbolic (or indefinite) dispersion are known as hyperbolic metamaterials (HMMs), where one of the principal components of the ε tensor is opposite in sign to the other two principal components.[4] The effective material dispersion of such metamaterials can be controlled by changing the amount of metal and dielectric materials forming the structure.[5] Some of the promising applications of HMM include optical hyperlenses which demonstrate far-field optical imaging beyond the diffraction limit,[6] near-perfect absorption,[7] abnormal scattering,[8] high-sensitivity sensors,[9] and long-range energy transfer.[10]

Additionally, HMMs provide an epsilon-near-zero (ENZ) feature where the real permittivity approaches zero at a certain wavelength range. The HMMs composed of alternating metal and dielectric thin layers have been demonstrated to exhibit ENZ behaviour in the designed wavelength region from visible to near-infrared[11–13] with the potential of ultrafast tuning of the permittivity.[14] This flexibility has extended the applications exhibited only by the naturally occurring ENZ materials to a broader range from plasmon–phonon coupling[15] and optical switching,[16] to non-resonant optical sensing[17] and the control of the localized surface plasmon resonances of nanoantennas.[18]

Another way of realizing certain effective electromagnetic responses, by all means, analogous to the metamaterials, is provided by the structural dispersion properties especially by the utilization of the waveguides. Engineering of the structural dispersion – where the optical properties depend on the geometry of the structure – has been studied in various waveguide designs.[19,20] One may define an effective relative permittivity for a guided mode in a waveguide. In other words, the dispersion of propagation inside a waveguide, for the fundamental mode, is equivalent to that of propagation in a medium with effective permittivity. Both rectangular waveguides and cylindrical waveguides have been identified to exhibit different fundamental waveguide modes with a cutoff frequency where the permittivity of the media is defined as approximately zero. This

M. Habib, I. Issah, H. Caglayan
Faculty of Engineering and Natural Sciences
Photonics
Tampere University
Tampere 33720, Finland
E-mail: humeyra.caglayan@tuni.fi
E. Bermúdez-Ureña
Centro de Investigación en Ciencia e Ingeniería de Materiales
and Escuela de Física
Universidad de Costa Rica
San José 11501, Costa Rica
The ORCID identification number(s) for the author(s) of this article can be found under https://doi.org/10.1002/adom.202200081.

DOI: 10.1002/adom.202200081

effective ENZ medium has shown promising relevance in loss reduction and strong coupling with emitters when embedded in it.[21–24] The entanglement of two qubits[25] and multiple qubits[26] were theoretically studied and show that ENZ medium provided by these waveguides support long-range entanglement. However, in order to realize this, a platform that facilitates the incorporation of quantum emitters while being compatible with multilayer fabrication steps is required.

The common and established technique to realize metamaterials with desired effective electromagnetic properties relies on the use of this material dispersion engineering. However, one can achieve unique applications by engineering structural dispersion as well as material dispersion. To this end, cylindrical HMMs can provide a feasible solution to investigate them in a single platform. Exploiting this for ENZ features may lead us to a remarkably simple design: a hollow circular structure formed with multilayer metamaterials which may act also as a waveguide.

In recent years, a non-traditional platform, the strained-induced rolled-up tubes (RUTs), has been investigated as a rapid and cost-efficient fabrication method for multilayer metamaterial structures.[27] Since the introduction of the RUT fabrication approach from planar thin films,[28] several fabrication methods have emerged,[29,30] enabling a wide variety of applications in different fields, from microelectronics and flexible devices,[31,32] to optics[33,34] and biology.[35,36] All of these methods exploit the residual strain gradients developed in different composition layers, which can undergo a stress-release driven self-rolling mechanism upon selective etching of a sacrificial layer. So far, most of the works on RUT metamaterials have focused on the possibility to stack optically active semiconductor heterostructures[37,38] and metallic nanostructures.[39,40] Moreover, Smith et al. pointed out that these RUTs can be promising candidates for waveguides[41] and hyperlenses.[42] Later these tubes were used for the realization of three-dimensional metamaterials,[43] fishnet HMMs,[44] and active metamaterials.[45] Initial RUT-based metamaterials had a predominant use of semiconductor layers grown by molecular beam epitaxy, which served both as the strained layers that drove the self-rolling process, as well as the dielectric material in the metamaterial structure.[27] The latter limited the operation wavelengths and material design flexibility of these structures, which in part limited exploring applications such as self-rolled ENZ-metamaterials. Over the past decade, the use of germanium (Ge) as a sacrificial layer was introduced, enabling the use of a wider range of materials in RUT fabrication, including common dielectrics that can be implemented for metamaterials operating at near-visible wavelengths.[30]

In this work, we implemented the Ge-based RUT fabrication approach to build self-rolled cylindrical multilayer structures to explore engineered ENZ metamaterials. We fabricated silicon dioxide/gold (SiO_2/Au)-based RUTs with different layer thickness combinations and diameters. Our optimized fabrication technique enabled tuning of the dispersion of the RUT in different regions of the visible and infrared (IR) range. Moreover, by bringing together a combination of experimental, theoretical, and numerical efforts, we demonstrate the structural and material-dependent dispersion of these RUTs with potential of exploiting ENZ features. By analytically modeling the diameters, and the material dispersion properties of RUTs considering the circular geometry, we rationalize the application of such structures in the field of metamaterials and plasmonics. Additionally, from the structure dispersion engineering aspect, this will provide the platform needed to observe quantum communication and nanophotonic applications based on the ENZ waveguide.

This unique platform for dispersion engineering and more specifically achieving ENZ metamaterials can open up very interesting applications which cannot be achievable with planar systems. For example, incorporation of quantum emitters and active materials and then rolling them to multiple layers for spontaneous emission enhancement and tunable ENZ metamaterials reduces the complex processes of incorporation and gating in multilayer structures to just one layer.

2. Self-Rolling Metamaterials

The fabrication approach for the SiO_2/Au-based RUTs is illustrated in **Figure 1**, which involves a two-step photolithography fabrication process combined with electron-beam-based layer deposition and lift-off to define the rolling areas. Initially, various sizes of rectangular Ge patterns (t = 40 nm) were defined on a silicon substrate, and this was followed by patterning and deposition of a smaller area to ensure the open edges required for the etching process from a $SiO_2(t_d)$/titanium (Ti)(t = 2 nm)/Au (t_m) layer sequence. The Ti layer was introduced as an adhesion layer between the SiO_2 and Au layers, and is not expected to influence the optical response of interest of the RUTs, as the imaginary part of the metal (i.e., losses) do not play a major role in the ENZ wavelength. In the final step, the Ge layer is selectively etched by immersing the sample in a H_2O_2 solution, which triggers the stress release-driven self-rolling process (see Section 6 for details).

The strain introduced between the layers arises from the fact that a slow deposition rate of SiO_2 induces compressive stress within the first layer while a relatively high deposition rate of Au creates tensile stress within the second layer. In addition to the deposition rate, the adhesive Ti layer under the Au layer can contribute to the strain.[46] Once this combination of films under stress is released by selectively etching the Ge layer, it results in the self-rolling of the films into a microtube (see Section 6 for details). Recently, a similar approach was implemented to demonstrate multilayered metasurfaces.[40]

Although it is possible to deposit different thickness layers, the strain between these layers is one of the important parameters that define the final RUT's diameter. Therefore, initially, we modelled the diameter of RUTs as a function of the thickness of the strained layers as:[47]

$$D = \frac{E_m^2 t_m^4 + E_d^2 t_d^4 + 4E_m E_d (t_m^3 t_d + t_m t_d^3) + 6E_m E_d (t_m^2 t_d^2)}{3\,|\Delta\xi|\,(1+\nu)E_m E_d (t_m + t_d)(t_m t_d)} \quad (1)$$

where, in this study, subscript m and d represent metal (Au) and dielectric (SiO_2), respectively, $\Delta\xi$ is the strain difference between the two layers, E is the Young's modulus, t is the thickness of films in nanometers (nm) and ν is the Poisson's ratio (set at 0.422). The E of Au was set at 79 GPa[48] and SiO_2 at 50 GPa.[49] The calculated diameter D of the RUTs as a function of the dielectric (t_d) and metal (t_m) thickness is presented

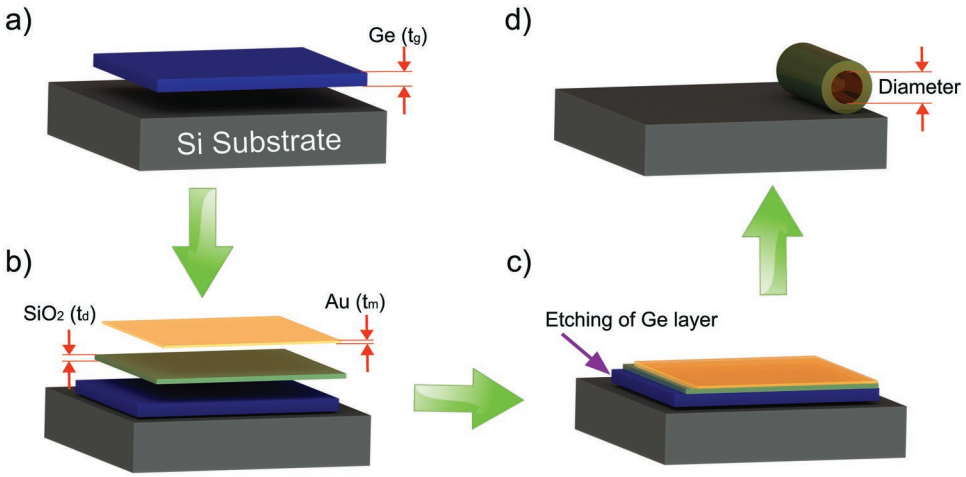

Figure 1. Schematic representation of the fabrication steps for obtaining RUTs. a) The first step consists of defining the Ge layer pattern. b) The second step opens a window to define the SiO_2 and Au bilayer, with reduced dimensions on the front and lateral sides in order to facilitate the next step, which is c) the etching process of the Ge, leading to the d) self-rolling of the SiO_2/Au layers into a RUT.

in **Figure 2**a, which contemplates SiO_2 and Au thickness ranges of 5–40 nm and 5–25 nm, respectively, encompassing the combinations of layer thicknesses of the experimental samples in this study. The analytically calculated diameter of the RUT, based on this model, shows that the thicker layers create larger diameters. To fit the model with experimentally measured diameters we consider an average of $\Delta\xi$ =1.2%.

In the systematic experimental study to identify the effect of different parameters on three-dimensional ENZ metamaterials, eight different samples were fabricated. We used four different dielectric thickness t_d (5 nm, 10 nm, 20 nm and 40 nm) and two different metal layer thickness t_m (10 nm and 20 nm). The scanning electron microscopy (SEM) images of the self-rolled structures at an angle of 40° are presented in Figure 2. We were able to achieve microtubes ranging from sub-micron diameters (≈0.63 µm) up to ≈7.5 µm. Note that the diameter of the RUTs depends on the strain, hence the thickness of SiO_2 and Au layers used to form the multilayer metamaterial.

In this fabrication process, the width (w_g) of rectangular pattern of Ge defines the length of the RUT, while the length (l_g) of the pattern controls the number of the turns (N). As N depends upon the diameter of the RUT through the fix area of the rectangular pattern, the number of turns can be approximated as a function of D and l_g as $N = l_g/\pi D$. In each sample, several pattern designs with varying length and width dimensions were included. The analysis of the results revealed that

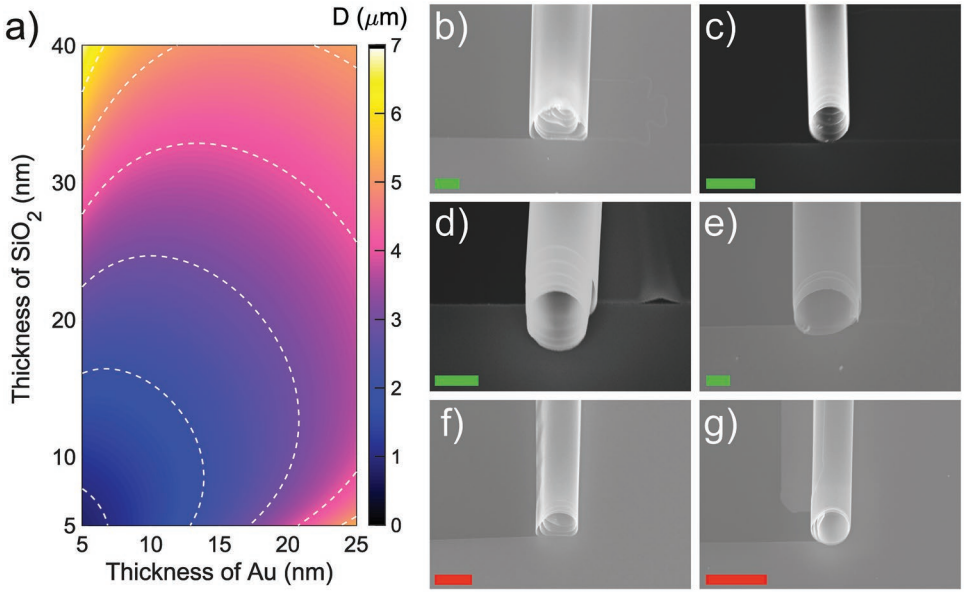

Figure 2. a) Analytically calculated diameter of a self-rolled structure as a function of Au and SiO_2 thicknesses, and SEM images of RUTs with b) t_d/t_m=5/20, c) t_d/t_m=10/10, d) t_d/t_m=20/10, e) t_d/t_m=20/20, f) t_d/t_m=40/10, and g) t_d/t_m=40/20 (all values in nm). The green scale bar is 2 µm and red one is 10 µm.

Table 1. Measured approximate inner diameters of the RUTs formed using corresponding t_d and t_m.

(t_m↓) (t_d→)	40 nm	20 nm	10 nm	5 nm
10 nm	7.5 μm (3)	2 μm (5)	712 nm (13)	632 nm (15)
20 nm	5 μm (5)	3 μm (3)	1250 nm (8)	1.5 μm (6)

the thin layers yield smaller diameters while the rolling success was better in smaller patterned areas. For example, the areas of 30×25 μm^2 ($w_g \times l_g$) provided compact RUTs with diameters below 3 μm, while areas of 90×75 μm^2 allowed proper rolling of the tubes with the diameters above 3 μm. **Table 1** presents the inner diameters from eight different samples, with the estimated number of turns they rolled given in parenthesis.

3. Material Dispersion of ENZ Multilayer Materials

Previously, the material dispersion of planar multilayer metamaterials has been qualitatively defined using the standard planar effective medium approximation (PEMA). This approximation method works based on the assumption that the number of layers is infinite and the effective permittivity is independent of the number of layers. Moreover, the metamaterial is considered as an infinite planar sheet and the dispersion is independent of the shape. However, due to these considerations in the PEMA method, the calculations may not be precisely suitable to describe the optical response of cylindrical HMMs with a finite number of SiO_2/Au layers. Therefore, in this study, we opted to implement a cylindrical effective medium approximation (CEMA) to define the effective dispersion properties of a curved multilayer medium.[50] **Figure 3**a shows a cross-section schematic of a cylindrical multilayer structure and the parameters defined in the model, with ε_ρ, ε_θ and ε_z as the principal permittivities in the ρ, θ and z directions, respectively in the cylindrical coordinate system.

In CEMA method, the effective permittivity values for the multilayer structures are expressed as:[50]

$$\varepsilon_\rho = \log(r_N/r_0)\left(\sum_{n=1}^{N}(\log(r_n/r_{n-1})/\varepsilon_n)\right)^{-1} \quad (2)$$

and

$$\varepsilon_\theta = \varepsilon_z = (\log(r_N/r_0))^{-1}\left(\sum_{n=1}^{N}(\log(r_n/r_{n-1})\varepsilon_n\right) \quad (3)$$

where the total number of layers are denoted by N. The innermost and outermost radii are denoted by (r_0) and (r_N), respectively. Each layer is defined by the radius (r_n) and permittivity (ε_n) corresponds to either ε_m and or ε_d which are the permittivity of Au and SiO_2. The thickness of each layer is $t_n = r_N - r_{n-1}$. This model takes into account the thicknesses of SiO_2/Au, the inner radius of the tube, and the number of turns, for example, number of bilayers. As discussed in the previous part, the thickness of the layers defines the diameter of a RUT. However, one advantage of the RUT fabrication approach is that one can obtain varying numbers of layers for fixed inner diameter and layer thickness values, which depend mainly on the length of the patterned area. In order to understand the effect of the number of turns, N and diameter on the dispersion, we calculate the real part of the effective permittivity values of ε_θ for 300 nm, 600 nm, and 900 nm diameters with different number of turns (see Figure S1, Supporting Information). The calculations revealed that the permittivity value does not depend on the number of turns when it is 4 or more. Hence, the use of

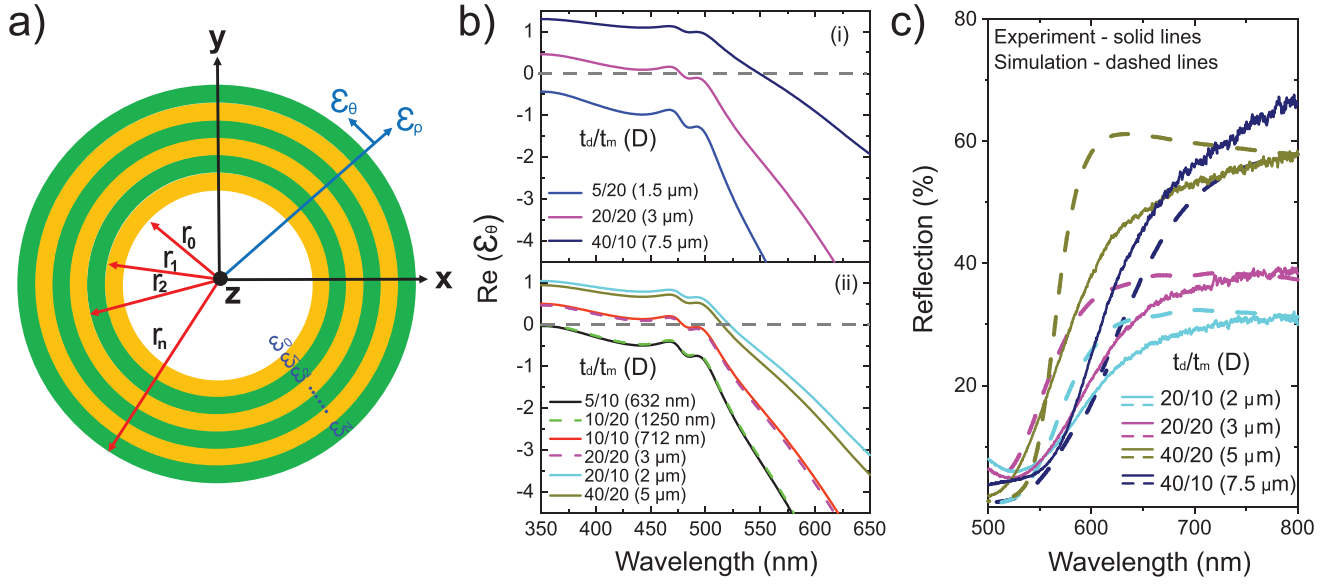

Figure 3. a) Schematic representation of a multilayer structure and corresponding permittivity values defined CEMA method. b) Calculated Re(ε_θ) of the fabricated RUTs using CEMA method. c) Simulated (dashed) and measured (solid) reflectance spectra from RUTs of diameters 2 μm (cyan), 3 μm (magenta), 5 μm (dark yellow) and 7.5 μm (navy blue).

CEMA for the samples presented in this work becomes particularly important when the RUTs have a number of turns less than 4 (e.g., RUTs with diameters 3 μm and 7.5 μm).

Next, we focus on the analysis of the dispersion of the fabricated samples. Figure 3b presents permittivity values for the fabricated RUTs based on the CEMA calculation by comparing the effect of ratio of the thicknesses of SiO_2 and Au (t_d/t_m), and also the diameter ($2r_0$). Figure 3b-i shows the dispersion of the RUTs with different thickness ratios [5/20, 20/20, and 40/10], presented by blue, magenta, and dark blue lines. The thickness of the layers defined the dispersion of the circular multilayer metamaterial. In addition, the large difference in the thickness ratios results in different diameters (1.5 μm, 3 μm, and 7.5 μm), as they provide different strain values but also modify the permittivity value and change the ENZ wavelength range quite significantly. Overall, the ENZ wavelength of the RUT is tuned from 400 to 600 nm, and it is possible to obtain the same or similar ENZ ranges using different diameters of RUTs by arranging the metal and dielectric layers.

Likewise, Figure 3b-ii shows Re(ε_θ) of some of the fabricated samples with identical thickness ratios (t_d/t_m) but different diameters (D). The dispersion results for 5/10 (632 nm) and 10/20 (1250 nm) as shown in black and green dotted lines, is identical although having different diameters. Similarly, Re(ε_θ) for 10/10 and 20/20 with diameter of 712 nm and 3 μm shown in red and dotted magenta lines, are almost identical. Whereas, the RUTs (2 μm and 5 μm) with a ratio of 20/10 and 40/20 have slightly different dispersion and ENZ wavelength regions. Note that, in all these tubes, the number of turns is more than 4, and the permittivity values are almost identical even though the thicknesses and diameter are different. The calculation of the material dispersion reveals that one can obtain quite similar results although the diameter of the RUT can be different. Therefore, one can design the ENZ wavelength range as well as the diameter based on the application needs such that it is possible to use a RUT with a diameter of 3 μm instead of 712 nm while exploiting the same material dispersion. Finally, we calculate the other three permittivity components for eight different RUTs using CEMA, presented in Figure S2, Supporting Information.

Furthermore, we investigate the reflectance response of some of the RUTs with sizes compatible with our measurement setup (see Section 6 for details). Figure 3c presents the simulation (dashed lines) and experimental (solid lines) for RUT with diameters of 2 μm (cyan), 3 μm (magenta), 5 μm (dark yellow) and 7.5 μm (navy blue). The results show the general trend for the reflection of the metamaterial with increasing reflectance above the ENZ wavelengths, that depends on the ε_θ when excited from the top along the longitudinal axis (γ-z plane). Our experimental results agree well with our simulated reflectance spectra within reasonable experimental deviations, which could arise either from the structure end (i.e., material properties and uniform compact stacking of the layers) as well as deviations in the measurement configuration compared to the idealized simulated structure. Furthermore, the reflection spectra of the RUTs with diameters of 2 μm and 5 μm confirm the modelled results in Figure 3b-ii, in that they exhibit a very similar ENZ transition (onset of the reflection band), however, the 5 μm RUT represents a more convenient platform for certain applications as it provides a larger area for the coupling to external optical elements.

4. Structural Dispersion of Circular ENZ Waveguides

Here, we explore the waveguide ENZ mode of the fabricated RUTs by taking advantage of structural dispersion. To study this dispersion phenomenon, we treated these samples as cylindrical waveguides and numerically implemented the Lumerical Finite-Difference Eigenmode (FDE) solver to calculate the spatial profile and frequency dependence of the excited modes of the waveguide. By solving Maxwell's equations on a cross-sectional mesh of the waveguide, we obtained the fundamental modes excited at the cutoff wavelength of the RUTs. We selected the fabricated RUTs with diameters (i.e., 632 nm, 712 nm, 1250 nm, and 1500 nm), and considering their dielectric-metal combination and number of turns, we compute their corresponding zero-index mode.

We initiated by studying the dispersion relation of the selected RUTs which exhibits the dependence of the waveguide effective mode indices n_{eff} as a function of wavelength. **Figure 4**a illustrates the structural dispersion relation of the RUT with different core diameters (D). This helped in identifying the cutoff wavelengths where the effective refractive index of the medium is approximately zero ($n_{eff} \approx 0$) for the different RUTs. Since the index of refraction is directly related to the permittivity, these structures exhibit effective ENZ features.

As the diameter of the RUT is the main defining parameter of the structural dispersion, for different diameters (i.e., 632 nm, 712 nm, 1250 nm, and 1500 nm), we obtained varied cutoff wavelengths of ≈1296 nm, ≈1488 nm, ≈2295 nm, and ≈2860 nm, respectively. This illustrates the dependence of the cutoff wavelength as a function of varying diameters of the selected RUTs where the cutoff wavelength redshifts with an increase in the diameter of the RUT. This illustrates the structural dispersion phenomena where a structural parameter such as the diameters of the RUT determines the zero-index mode that can be excited in the RUT (Figure 4b). Note that a circular waveguide structure, similar to our RUTs, illustrates a fundamental (TE_{11}) mode at their corresponding cutoff wavelengths. At the cutoff wavelength the TE_{11} mode of the RUT has a dispersion curve that begins at the light line and cuts off the wavelength axis at $k = 0$. A wave vector that is vanishingly small at the cutoff wavelength implies a waveguide mode with a near-zero index ($n_{eff} = k/k_0$) where the wave displays little or no spatial variations. Overall, these waveguide structures around the cutoff frequency of its fundamental mode behave as a metamaterial with an effective ENZ features.

5. Conclusion and Outlook

In conclusion, we have studied the SiO_2/Au based self-rolling RUTs, and identified the material and structural dispersion of circular multilayer metamaterials. We fabricated RUTs with diameters ranging from ≈0.6 μm to 7.5 μm using different metal and dielectric layer thicknesses. We qualitatively define

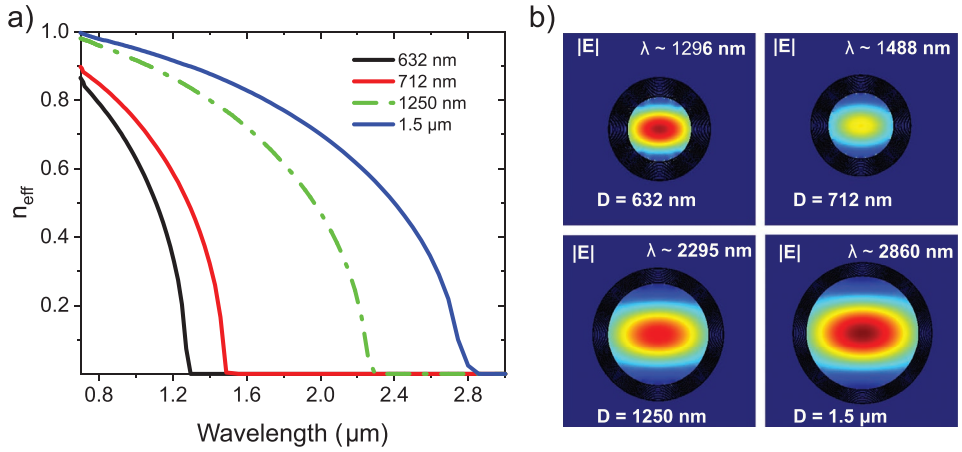

Figure 4. a) The dependence of the waveguide mode effective indices n_{eff} on the wavelengths for the selected diameters. b) Fundamental TE_{11} electric field |E| distribution for the selected diameters of the RUT at their corresponding cutoff wavelength.

the optical dispersion of these circular multilayer structures using an effective medium approximation method. This analytical model reveals that the ENZ wavelength range of RUTs can be tuned by the ratio of the metal and dielectric content. However, the diameter of the RUT which is also a parameter in these calculations is interrelated to the thicknesses of the layers and their ratio via the strain-induced fabrication method. Hence, it is possible to obtain similar dispersion properties for RUTs with different diameters but similar thickness ratios. We showed that the fabricated RUTs in this study exhibit ENZ wavelengths in the visible range for various diameters. We have also characterized and numerically obtained the reflection response of the RUTs with a diameter bigger than 1.5 μm to confirm the dispersion about via the model. In the next section, we focused on the structural dispersion by considering the fabricated RUTs as cylindrical waveguides. We numerically calculated the waveguide modes supported inside the core of the RUTs and identified the cutoff wavelength of the fundamental mode which supports the ENZ medium. We observed a strong shift in the cut-off wavelength from 1296 nm to 2860 nm for RUTs with diameters ranging from ~0.6 μm to 1.5 μm, respectively. This makes the ENZ mode very sensitive to the diameter of the RUT.

Overall, we propose a self-rolling ENZ medium whose optical properties can be engineered through material and structural dispersion. Therefore, this work opens new applications for ENZ metamaterials, such as studying the integration of phase-changing materials on a planar layer and rolling them to form multilayer tunable ENZ (e.g., graphene and vanadium dioxide). Moreover, the integration of quantum emitters in an ENZ medium can be used for quantum information processing and communication applications.

6. Methods

6.1. Fabrication

For the fabrication of RUT, the 500 μm thick silicon (Si) substrate was cleaned in acetone and later isopropanol (IPA) with 10 min of sonication for each solvent and blow dried under nitrogen (N_2) flow. Once the samples are thoroughly cleaned, we performed image reversal lithography for Ge patterning. The samples were coated with a thin layer of Hexamethyldisilazane (HMDS) at 125 °C to improve the adhesion of the photolithography resist. AZ5214E resist was spin-coated at 3000 revolutions per minute (RPM) for 40 s. The resist was soft baked at 100 °C for 60 s. The spin-coated samples were exposed using the Suss MA6 mask aligner for 4 s under an UV lamp using the rectangular pattern in the mask. The post-baking process was done at 115 °C for 120 s. For image reversal the samples were exposed second time without mask using same Suss MA6 mask aligner for 30 s. The samples were developed for 45 s using MIF 726 developer and then rinsed three times in di-ionized (DI) water. The developed samples were coated with 40 nm of Ge. The S-1165 remover was used to lift off the unwanted metal, the samples were left in the solution to heat up to 80 °C. When the desired temperature was reached, the hot plate was turned off and the samples were sonicated in the solution for 5 min. The sample was rinsed in water, acetone and IPA, and blow dried under N_2 flow to get rid of residual metal film. We further cleaned the resist residue by reactive ion etching (RIE) with oxygen (O_2) plasma for 2 min. The quality of Ge patterns was verified using a microscope.

Once Ge patterns were obtained, we performed second step lithography using positive resist to create an opening for Ge etching. We started with the same parameters for HMDS adhesion layer. Then, AZ3421E resist was spin-coated at 3000 RPM for 40 s. The resist was soft baked at 90 °C for 90 s. The spin-coated samples were exposed using the Suss MA6 mask aligner for 4 s. The post-baking process was done at 110 °C for 60 s. The samples were developed for 60 sec using MIF 726 developer and then rinsed three times in DI water. The developed samples were then coated with SiO_2 at 0.1 nm/s and Ti/Au at 0.3 nm with different thickness combinations. Au were deposited at an angle of 60°, to further guide the rolling direction. Once the samples were coated, the lift-off was done by using S1165 remover, which opened the window for the wet etching of Ge. The etching was done by leaving the samples in 35% of H_2O_2 for 90 min. We etched Ge layer, that allowed the rolling

of the strained SiO_2/Au layers. SEM images are presented in Figure 2.

6.2. Numerical Simulations

The optical response of RUTs is numerically calculated using Ansys Lumerical FDTD Solutions. 3D electromagnetic simulations of reflection were performed using a plane wave source. The size of the simulation region was defined based on the maximum diameter of the RUT. The complex refractive index of the Au and SiO_2 used in the simulation is from the material data of Johnson and Christy,[51] and Palik,[52] respectively. To obtain the optical response of RUTs with different diameter, we set our boundary conditions to perfectly matched layer (PML) along the *x*, *y*, and *z* axes with increased number of PML layers. A conformal mesh of 4 nm is used in the simulation region while a finer mesh of 2 nm is employed in the region enclosing the RUTs to get better resolution.

The fundamental mode profiles and structural dispersion of the RUT were characterized using a Finite Difference Eigenmode (FDE) solver in Ansys Lumerical MODE. The numerical simulation was set up by building up different thickness-dependent alternating layers of SiO_2 and Au with a hollow air core using Ansys Lumerical script commands. The solver type is set to 2D normal to calculate the mode profiles that exist in the RUT in the x-y plane. We used a minimum mesh step of 0.001 nm, grading factor of $\sqrt{2}$ and conformer variant 1 mesh refinement to attain mode profiles with good resolution.

The mode profiles and the cutoff wavelength of the rolled-up waveguide were determined for different selected core diameters (D) (i.e., 632 nm, 712 nm, 1250 nm, and 1500 nm). In addition, parametric sweeps of the fundamental (TE_{11}) mode at different spectral wavelengths were implemented for the different diameters of the waveguide to obtain their corresponding effective index (n_{eff}). The structural dispersion relation of the selected RUT diameters is presented as the relation between the effective index (n_{eff}) and the cutoff wavelengths of the RUT structure. We calculated the material dispersion relation of the RUT using an in-house developed MATLAB code based on the CEMA formulations.

6.3. Optical Characterization

The reflectance spectrum of the RUTs is measured using a confocal Raman microscope (WiTec alpha300R). The samples were excited by a broadband light source and the beam was focused to tube top curvature of RUTs using a 100x air objective with NA of 0.9. The same objective was used to collect the reflected signal in the normal direction. The excitation and collection beam spot was of ≈1.2 µm. The measured reflectance of the RUTs was normalized against that of a silver (Ag) mirror.

Supporting Information

Supporting Information is available from the Wiley Online Library or from the author.

Acknowledgements

The authors thank Daria Briukhanova for the support on the fabrication process. The authors acknowledge the financial support of the European Research Council (Starting Grant project aQUARiUM; Agreement No. 802986) and Academy of Finland Flagship Programme (PREIN) (320165).

Conflict of Interest

The authors declare no conflict of interest.

Data Availability Statement

The data that support the findings of this study are available from the corresponding author upon reasonable request.

Keywords

effective medium approximation, epsilon-near-zero, metamaterials, rolled-up tubes

Received: January 13, 2022
Revised: April 19, 2022
Published online:

[1] T. J. Cui, D. R. Smith, R. Liu, *Metamaterials*, Springer, Berlin Heidelberg **2010**.
[2] N. Engheta, R. W. Ziolkowski, *Metamaterials: Physics and Engineering Explorations*, John Wiley & Sons, Hoboken, NJ **2006**.
[3] I. Liberal, A. M. Mahmoud, Y. Li, B. Edwards, N. Engheta, *Science* **2017**, *355*, 1058.
[4] L. Ferrari, C. Wu, D. Lepage, X. Zhang, Z. Liu, *Prog. Quantum Electron.* **2015**, *40*, 1.
[5] A. Poddubny, I. Iorsh, P. Belov, Y. Kivshar, *Nat. Phot.* **2013**, *7*, 948.
[6] Z. Jacob, L. V. Alekseyev, E. Narimanov, *Opt. Express* **2006**, *14*, 8247.
[7] N. Maccaferri, Y. Zhao, T. Isoniemi, M. Iarossi, A. Parracino, G. Strangi, F. De Angelis, *Nano Lett.* **2019**, *19*, 1851.
[8] C. Qian, X. Lin, Y. Yang, F. Gao, Y. Shen, J. Lopez, I. Kaminer, B. Zhang, E. Li, M. Soljačić, H. Chen, *ACS Photonics* **2018**, *5*, 1506.
[9] K. V. Sreekanth, P. Mahalakshmi, S. Han, M. S. Mani Rajan, P. K. Choudhury, R. Singh, *Adv. Opt. Mater.* **2019**, *7*, 1900680.
[10] C. L. Cortes, Z. Jacob, *Nat. Commun.* **2017**, *8*, 14144.
[11] R. Maas, J. Parsons, N. Engheta, A. Polman, *Nat. Phot.* **2013**, *7*, 907.
[12] J. Gao, L. Sun, H. Deng, C. J. Mathai, S. Gangopadhyay, X. Yang, *Appl. Phys. Lett.* **2013**, *103*, 051111.
[13] K. V. Sreekanth, A. De Luca, G. Strangi, *Sci. Rep.* **2013**, *3*, 1.
[14] A. R. Rashed, B. C. Yildiz, S. R. Ayyagari, H. Caglayan, *Phys. Rev. B* **2020**, *101*, 165301.
[15] D. Yoo, F. de León-Pérez, M. Pelton, I.-H. Lee, D. A. Mohr, M. B. Raschke, J. D. Caldwell, L. Martín-Moreno, S.-H. Oh, *Nat. Phot.* **2021**, *15*, 125.
[16] J. Bohn, T. S. Luk, C. Tollerton, S. W. Hutchings, I. Brener, S. Horsley, W. L. Barnes, E. Hendry, *Nat. Commun.* **2021**, *12*, 1017.
[17] Z. Fusco, M. Taheri, R. Bo, T. Tran-Phu, H. Chen, X. Guo, Y. Zhu, T. Tsuzuki, T. P. White, A. Tricoli, *Nano Lett.* **2020**, *20*, 3970.
[18] M. Habib, D. Briukhanova, N. Das, B. C. Yildiz, H. Caglayan, *Nanophotonics* **2020**, *9*, 3637.
[19] E. J. R. Vesseur, T. Coenen, H. Caglayan, N. Engheta, A. Polman, *Phys. Rev. Lett.* **2013**, *110*, 013902.

[20] B. Edwards, A. Alù, M. E. Young, M. Silveirinha, N. Engheta, *Phys. Rev. Lett.* **2008**, *100*, 033903.
[21] I. Issah, M. Habib, H. Caglayan, *Nanophotonics* **2021**, *10*, 4579.
[22] B. C. Yildiz, H. Caglayan, *Phys. Rev. B* **2020**, *102*, 165303.
[23] Y. Li, I. Liberal, N. Engheta, *Sci. Adv.* **2019**, *5*, eaav3764.
[24] Y. Li, C. Argyropoulos, *Opt. Lett.* **2018**, *43*, 1806.
[25] I. Issah, H. Caglayan, *Appl. Phys. Lett.* **2021**, *119*, 221103.
[26] Y. Li, C. Argyropoulos, *Appl. Phys. Lett.* **2021**, *119*, 211104.
[27] S. Schwaiger, A. Rottler, S. Mendach, *Adv. Opto Electron.* **2012**, *2012*, 1.
[28] V. Y. Prinz, V. A. Seleznev, A. K. Gutakovsky, A. V. Chehovskiy, V. V. Preobrazhenskii, M. A. Putyato, T. A. Gavrilova, *Phys. E* **2000**, *6*, 828.
[29] Y. Mei, G. Huang, A. A. Solovev, E. Bermúdez-Ureña, I. Mönch, F. Ding, T. Reindl, R. K. Fu, P. K. Chu, O. G. Schmidt, *Adv. Mater.* **2008**, *20*, 4085.
[30] C. C. Bof Bufon, J. D. Cojal González, D. J. Thurmer, D. Grimm, M. Bauer, O. G. Schmidt, *Nano Lett.* **2010**, *10*, 2506.
[31] W. Huang, M. Li, S. Gong, X. Li, in *2015 73rd Annual Device Research Conference (DRC)* **2015**, pp. 223–224.
[32] V. K. Bandari, Y. Nan, D. Karnaushenko, Y. Hong, B. Sun, F. Striggow, D. D. Karnaushenko, C. Becker, M. Faghih, M. Medina-Sánchez, *Nat. Electron.* **2020**, *3*, 172.
[33] C. Strelow, S. Kietzmann, A. Schramm, R. Seher, J.-P. Penttinen, T. V. Hakkarainen, A. Mews, T. Kipp, *Appl. Phys. Lett.* **2012**, *101*, 113114.
[34] Y. Zhang, D. Han, D. Du, G. Huang, T. Qiu, Y. Mei, *Plasmonics* **2015**, *10*, 949.
[35] C. K. Schmidt, M. Medina-Sánchez, R. J. Edmondson, O. G. Schmidt, *Nat. Commun.* **2020**, *11*, 5618.
[36] O. V. Cangellaris, E. A. Corbin, P. Froeter, J. A. Michaels, X. Li, M. U. Gillette, *ACS Appl. Mater. Interfaces* **2018**, *10*, 35705.
[37] K. M. Schulz, H. Vu, S. Schwaiger, A. Rottler, T. Korn, D. Sonnenberg, T. Kipp, S. Mendach, *Phys. Rev. Lett.* **2016**, *117*, 085503.
[38] S. Kietzmann, C. Strelow, L. Tavares, J.-P. Penttinen, T. V. Hakkarainen, A. Schramm, A. Osadnik, A. Lutzen, J. Kjelstrup-Hansen, A. Mews, *ACS Photonics* **2015**, *2*, 1532.
[39] H. Vu, J. Siebels, D. Sonnenberg, S. Mendach, T. Kipp, *ACS Photonics* **2017**, *4*, 2659.
[40] E. Bermúdez-Ureña, U. Steiner, *ACS Photonics* **2019**, *6*, 2198.
[41] E. J. Smith, Z. Liu, Y. Mei, O. G. Schmidt, *Nano Lett.* **2010**, *10*, 1.
[42] E. J. Smith, Z. Liu, Y. F. Mei, O. G. Schmidt, *Appl. Phys. Lett.* **2009**, *95*, 083104.
[43] S. Schwaiger, M. Bröll, A. Krohn, A. Stemmann, C. Heyn, Y. Stark, D. Stickler, D. Heitmann, S. Mendach, *Phys. Rev. Lett.* **2009**, *102*, 163903.
[44] D. Briukhanova, M. Habib, I. Issah, H. Caglayan, *Appl. Phys. Lett.* **2021**, *119*, 141101.
[45] S. Schwaiger, M. Klingbeil, J. Kerbst, A. Rottler, R. Costa, A. Koitmäe, M. Bröll, C. Heyn, Y. Stark, D. Heitmann, *Phys. Rev. B* **2011**, *84*, 155325.
[46] M. Habib, I. Issah, D. Briukhanova, A. R. Rashed, H. Caglayan, *ACS Appl. Nano Mater.* **2021**, *4*, 8699.
[47] S. M. Harazim, W. Xi, C. K. Schmidt, S. Sanchez, O. G. Schmidt, *J. Mater. Chem.* **2012**, *22*, 2878.
[48] Y. Y. Kim, *Materials* **2017**, *10*, 806.
[49] C. Ho, A. Dehoux, L. Lacroix, J. Alexis, O. Dalverny, S. Châtel, B. Faure, *International Journal of Engineering Research & Science* **2018**, *4*, 38.
[50] R. Kumar, K. Kajikawa, *J. Opt. Soc. Am. B* **2019**, *36*, 559.
[51] P. B. Johnson, R.-W. Christy, *Phys. Rev. B* **1972**, *6*, 4370.
[52] I. H. Malitson, *J. Opt. Soc. Am.* **1965**, *55*, 1205.